Article:
Adlarson, P., Augustyniak, W., Bardan, W. et al. (47 more authors) (2018) Total and differential cross sections of η-production in proton–deuteron fusion for excess energies between Qη = 13 MeV and Qη = 81 MeV. Physics Letters, Section B: Nuclear, Elementary Particle and High-Energy Physics. pp. 297-304. ISSN 0370-2693

https://doi.org/10.1016/j.physletb.2018.05.036

Physics Letters B 782 (2018) 297–304

Contents lists available at ScienceDirect

Physics Letters B

www.elsevier.com/locate/physletb

Total and differential cross sections of η-production in proton–deuteron fusion for excess energies between $Q_\eta = 13$ MeV and $Q_\eta = 81$ MeV

The WASA-at-COSY Collaboration

P. Adlarson [a], W. Augustyniak [b], W. Bardan [c], M. Bashkanov [d], F.S. Bergmann [e], M. Berłowski [f], A. Bondar [g,h], M. Büscher [i,j], H. Calén [a], I. Ciepał [k], H. Clement [l,m], E. Czerwiński [c], K. Demmich [e], R. Engels [n], A. Erven [o], W. Erven [o], W. Eyrich [p], P. Fedorets [n,q], K. Föhl [r], K. Fransson [a], F. Goldenbaum [n], A. Goswami [n,s], K. Grigoryev [n,t], C.-O. Gullström [a], L. Heijkenskjöld [a,1], V. Hejny [n], N. Hüsken [e,*], L. Jarczyk [c], T. Johansson [a], B. Kamys [c], G. Kemmerling [o,2], G. Khatri [c,3], A. Khoukaz [e], A. Khreptak [c], D.A. Kirillov [u], S. Kistryn [c], H. Kleines [o,2], B. Kłos [v], W. Krzemień [f], P. Kulessa [k], A. Kupść [a,f], A. Kuzmin [g,h], K. Lalwani [w], D. Lersch [n], B. Lorentz [n], A. Magiera [c], R. Maier [n,x], P. Marciniewski [a], B. Mariański [b], H.-P. Morsch [b], P. Moskal [c], H. Ohm [n], W. Parol [k], E. Perez del Rio [l,m,4], N.M. Piskunov [u], D. Prasuhn [n], D. Pszczel [a,f], K. Pysz [k], A. Pyszniak [a,c], J. Ritman [n,x,y], A. Roy [s], Z. Rudy [c], O. Rundel [c], S. Sawant [z], S. Schadmand [n], I. Schätti-Ozerianska [c], T. Sefzick [n], V. Serdyuk [n], B. Shwartz [g,h], K. Sitterberg [e], T. Skorodko [l,m,aa], M. Skurzok [c], J. Smyrski [c], V. Sopov [q], R. Stassen [n], J. Stepaniak [f], E. Stephan [v], G. Sterzenbach [n], H. Stockhorst [n], H. Ströher [n,x], A. Szczurek [k], A. Trzciński [b], M. Wolke [a], A. Wrońska [c], P. Wüstner [o], A. Yamamoto [ab], J. Zabierowski [ac], M.J. Zieliński [c], J. Złomańczuk [a], P. Żuprański [b], M. Żurek [n], C. Wilkin [ad]

[a] Division of Nuclear Physics, Department of Physics and Astronomy, Uppsala University, Box 516, 75120 Uppsala, Sweden
[b] Department of Nuclear Physics, National Centre for Nuclear Research, ul. Hoza 69, 00-681, Warsaw, Poland
[c] Institute of Physics, Jagiellonian University, Prof. Stanisława Łojasiewicza 11, 30-348 Kraków, Poland
[d] School of Physics and Astronomy, University of Edinburgh, James Clerk Maxwell Building, Peter Guthrie Tait Road, Edinburgh EH9 3FD, United Kingdom
[e] Institut für Kernphysik, Westfälische Wilhelms-Universität Münster, Wilhelm-Klemm-Str. 9, 48149 Münster, Germany
[f] High Energy Physics Department, National Centre for Nuclear Research, ul. Hoza 69, 00-681, Warsaw, Poland
[g] Budker Institute of Nuclear Physics of SB RAS, 11 akademika Lavrentieva prospect, Novosibirsk, 630090, Russia
[h] Novosibirsk State University, 2 Pirogova Str., Novosibirsk, 630090, Russia
[i] Peter Grünberg Institut, PGI-6 Elektronische Eigenschaften, Forschungszentrum Jülich, 52425 Jülich, Germany
[j] Institut für Laser- und Plasmaphysik, Heinrich-Heine Universität Düsseldorf, Universitätsstr. 1, 40225 Düsseldorf, Germany
[k] The Henryk Niewodniczański Institute of Nuclear Physics, Polish Academy of Sciences, Radzikowskiego 152, 31-342 Kraków, Poland
[l] Physikalisches Institut, Eberhard-Karls-Universität Tübingen, Auf der Morgenstelle 14, 72076 Tübingen, Germany
[m] Kepler Center für Astro- und Teilchenphysik, Physikalisches Institut der Universität Tübingen, Auf der Morgenstelle 14, 72076 Tübingen, Germany
[n] Institut für Kernphysik, Forschungszentrum Jülich, 52425 Jülich, Germany
[o] Zentralinstitut für Engineering, Elektronik und Analytik, Forschungszentrum Jülich, 52425 Jülich, Germany
[p] Physikalisches Institut, Friedrich-Alexander-Universität Erlangen-Nürnberg, Erwin-Rommel-Str. 1, 91058 Erlangen, Germany
[q] Institute for Theoretical and Experimental Physics named after A.I. Alikhanov of National Research Centre "Kurchatov Institute", 25 Bolshaya Cheremushkinskaya, Moscow, 117218, Russia
[r] II. Physikalisches Institut, Justus-Liebig-Universität Gießen, Heinrich-Buff-Ring 16, 35392 Giessen, Germany
[s] Department of Physics, Indian Institute of Technology Indore, Khandwa Road, Simrol, Indore 453552, Madhya Pradesh, India

* Corresponding author.
E-mail address: n_hues02@uni-muenster.de (N. Hüsken).

[1] Present address: Institut für Kernphysik, Johannes Gutenberg-Universität Mainz, Johann-Joachim-Becher Weg 45, 55128 Mainz, Germany.
[2] Present address: Jülich Centre for Neutron Science JCNS, Forschungszentrum Jülich, 52425 Jülich, Germany.
[3] Present address: Department of Physics, Harvard University, 17 Oxford St., Cambridge, MA 02138, USA.
[4] Present address: INFN, Laboratori Nazionali di Frascati, Via E. Fermi, 40, 00044 Frascati (Roma), Italy.

https://doi.org/10.1016/j.physletb.2018.05.036

[t] High Energy Physics Division, Petersburg Nuclear Physics Institute named after B.P. Konstantinov of National Research Centre "Kurchatov Institute", 1 mkr. Orlova roshcha, Leningradskaya Oblast, Gatchina, 188300, Russia
[u] Veksler and Baldin Laboratory of High Energiy Physics, Joint Institute for Nuclear Physics, 6 Joliot-Curie, Dubna, 141980, Russia
[v] August Chełkowski Institute of Physics, University of Silesia, Uniwersytecka 4, 40-007, Katowice, Poland
[w] Department of Physics, Malaviya National Institute of Technology Jaipur, JLN Marg Jaipur 302017, Rajasthan, India
[x] JARA-FAME, Jülich Aachen Research Alliance, Forschungszentrum Jülich, 52425 Jülich and RWTH Aachen, 52056 Aachen, Germany
[y] Institut für Experimentalphysik I, Ruhr-Universität Bochum, Universitätsstr. 150, 44780 Bochum, Germany
[z] Department of Physics, Indian Institute of Technology Bombay, Powai, Mumbai 400076, Maharashtra, India
[aa] Department of Physics, Tomsk State University, 36 Lenina Avenue, Tomsk, 634050, Russia
[ab] High Energy Accelerator Research Organisation KEK, Tsukuba, Ibaraki 305-0801, Japan
[ac] Astrophysics Division, National Centre for Nuclear Research, Box 447, 90-950 Łódź, Poland
[ad] Physics and Astronomy Department, UCL, Gower Street, London WC1E 6BT, United Kingdom

ARTICLE INFO

Article history:
Received 20 January 2018
Received in revised form 23 April 2018
Accepted 13 May 2018
Available online 18 May 2018
Editor: V. Metag

Keywords:
Meson production
Proton–deuteron interactions
η meson

ABSTRACT

New data on both total and differential cross sections of the production of η mesons in proton–deuteron fusion to ^{3}He$\,\eta$ in the excess energy region 13.6 MeV $\leq Q_\eta \leq$ 80.9 MeV are presented. These data have been obtained with the WASA-at-COSY detector setup located at the Forschungszentrum Jülich, using a proton beam at 15 different beam momenta between $p_p = 1.60$ GeV/c and $p_p = 1.74$ GeV/c. While significant structure of the total cross section is observed in the energy region 20 MeV $\lesssim Q_\eta \lesssim$ 60 MeV, a previously reported sharp variation around $Q_\eta \approx 50$ MeV cannot be confirmed. Angular distributions show the typical forward-peaking that was noted earlier. For the first time, it is possible to study the development of these angular distributions with rising excess energy over a wide interval.

1. Introduction

The production of η mesons off nuclei has been a topic of active research over at least two decades. Inspired by the attractive interaction between η mesons and nuclei, first studied by Bhalerao, Haider and Liu [1,2], extensive experimental effort was put into the study of near-threshold production of η mesons off various nuclei. Although the original work suggested studies on heavier nuclei, already the η production off light nuclei such as the deuteron [3–6], ^{3}He or ^{4}He [7,8] revealed signs of a strong final state interaction. The reaction $pd \to {}^3\mathrm{He}\,\eta$ is one of the most discussed due to its markedly enhanced cross section very close to the production threshold, a feature that can also be found in photoproduction of η mesons off ^{3}He [9,10]. In proton–deuteron fusion, it was observed that the production cross section σ rises from zero at threshold to around 400 nb within less than 1 MeV of excess energy [11–14]. This curious behaviour of the production cross section has first been discussed in the context of a strong final state interaction and the presence of a possible (quasi-)bound η^3He state close to the threshold in [15], which was later followed up on, e.g., in [16,17]. However, while the production cross section of the reaction $pd \to {}^3\mathrm{He}\,\eta$ has been studied in great detail close to threshold, at higher excess energies the available database becomes sparse. Measurements by the CELSIUS/WASA [18], COSY-11 [19] and ANKE [20] groups seem to suggest a cross section plateau away from threshold, whereas a measurement by the GEM collaboration [21] yielded a larger cross section, albeit with a sizable uncertainty.

A sharp variation of the total cross section between $Q_\eta =$ 48.8 MeV and $Q_\eta = 59.8$ MeV has recently been reported [22]. In order to investigate further the existence and cause of this cross section variation, a new measurement was performed at 15 different beam momenta between $p_p = 1.60$ GeV/c and $p_p =$ 1.74 GeV/c, using the experimental apparatus WASA at the COoler SYnchrotron COSY. Apart from determining the total cross section of the proton–deuteron fusion to the ^{3}He$\,\eta$ final state, the focus of the new measurement is on the precise determination of differential cross sections and the study of their development with rising excess energy. Such a comparison between differential distributions at different excess energies has thus far been hindered by large systematic differences between the individual measurements performed in the various experiments mentioned above. For this reason, a consistent measurement over a wide range of higher excess energies in a single experiment allows for the first time an in-depth study of the dependence of the differential cross section on the excess energy. High quality data are of great importance in order to facilitate theoretical work on the production mechanism of η mesons in proton–deuteron fusion, as has recently been claimed in [23]. Up to now, no model exists that manages to correctly reproduce the total and differential cross sections away from the production threshold. While the two-step model, first studied by [24] in a classical framework and by [25] quantum-mechanically, has some success in describing near-threshold data (see, e.g., [23,25]), at larger excess energies the model no longer describes the available data [26,27].

In [28], it was claimed that the GEM data can be adequately described by a resonance model, in which η mesons are produced from the decay of a N^* resonance. Such a model is, however, unlikely to have a large contribution close to threshold due to the large momentum transfer necessary to compensate for the η meson mass. It remains to be seen if the production mechanism of the reaction $pd \to {}^3\mathrm{He}\,\eta$ changes with energy and, if so, why. It is for these reasons that in [23] new data at larger excess energies were assessed to be of high priority.

2. Experiment

The measurement was performed using the WASA detector setup (which is described in detail in [29]) at the storage ring COSY of the Forschungszentrum Jülich. Utilizing the so-called supercycle mode of the storage ring, the momenta of the beam protons are changed at each injection of a new proton bunch. Eight beam settings can be stored at once and the measurement was composed of two such supercycles (SC), each containing the eight beam momenta (flat-tops) indicated in Table 1. In total, data were taken at 15 different beam momenta between $p_p = 1.60$ GeV/c and $p_p =$

Table 1
Nominal beam momenta p_p for each supercycle and flat-top in GeV/c.

	FT0	FT1	FT2	FT3	FT4	FT5	FT6	FT7
SC0	1.60	1.62	1.64	1.66	1.68	1.70	1.72	1.74
SC1	1.61	1.63	1.65	1.67	1.69	1.70	1.71	1.73
SC2						1.70		

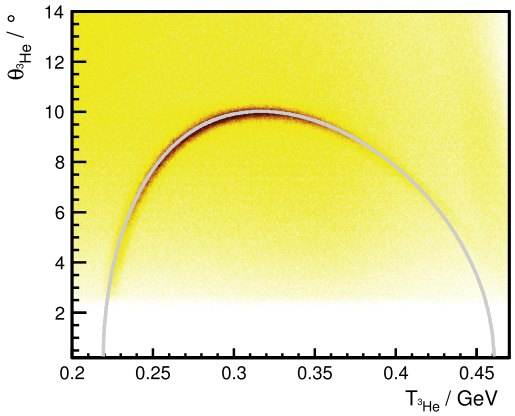

Fig. 1. Distribution of polar angle $\theta_{^3\mathrm{He}}$ versus kinetic energy $T_{^3\mathrm{He}}$ of ^{3}He candidates stopped in the first layer of the WASA Forward Range Hodoscope from the measurement at $p_p = 1.70$ GeV/c. The grey line shows the kinematical expectation for the reaction $pd \to {}^3\mathrm{He}\,\eta$ at $p_p = 1.70$ GeV/c, whereas the colour of the histograms reflects the number of reconstructed ^{3}He nuclei. (For interpretation of the colours in the figure(s), the reader is referred to the web version of this article.)

1.74 GeV/c with a momentum spread of around $\Delta p/p = 10^{-3}$ [30] and a stepsize of 10 MeV/c. The measurement at a momentum of $p_p = 1.70$ GeV/c was repeated in both supercycles and in an additional single-energy measurement for systematic checks. Inside the WASA Central Detector the beam protons are steered to collide with a deuterium pellet target. Due to the fixed-target geometry, heavy ejectiles like ^{3}He are produced near the forward direction and subsequently stopped inside the WASA Forward Detector. Here, using a proportional chamber and various layers of plastic scintillator, both the production angles θ and φ, and the energy deposit of forward-going particles are reconstructed. Doubly-charged Helium ions can be efficiently separated from protons, deuterons and charged pions by their energy deposit. From the deposited energy, the kinetic energy of ^{3}He nuclei is also evaluated, thus, in combination with the determined scattering angles, fully reconstructing their four-momenta.

3. Data analysis

For a two-particle final state such as $^3\mathrm{He}\,\eta$, the polar angle $\theta_{^3\mathrm{He}}$ and the kinetic energy $T_{^3\mathrm{He}}$ of the Helium nuclei are kinematically correlated. Using this relation, the precise measurement of the polar angle $\theta_{^3\mathrm{He}}$ ($\Delta\theta_{^3\mathrm{He}} \approx 0.2°$) can be exploited to give a very accurate calibration of the reconstructed energy. A comparison of the two-dimensional distribution of $\theta_{^3\mathrm{He}}$ versus $T_{^3\mathrm{He}}$ between the kinematical expectation for the signal reaction $pd \to {}^3\mathrm{He}\,\eta$ and the data obtained at $p_p = 1.70$ GeV/c can be found in Fig. 1.

The reaction of interest is identified from the spectra of the final state momentum of ^{3}He nuclei in the centre-of-mass frame $p^*_{^3\mathrm{He}}$ in a missing-mass analysis. Thus, no assumption on the η decay is made. Dividing the cosine of the centre-of-mass scattering angle $\cos\theta^*_\eta$ into 100 equally sized bins, the final state momentum spectra are fitted by a background function, excluding the peak region. Here, the background is a sum of Monte Carlo (MC) simulations of two- and three-pion production as well as a third order polynomial, accounting both for other possible background reactions and deviations from simple phase space distributions in the case of the three-pion production. The simulation of two-pion production was performed using a model incorporating the ABC effect and t-channel double-$\Delta(1232)$ excitation, developed for [31]. An example of such a fit can be found in Fig. 2.

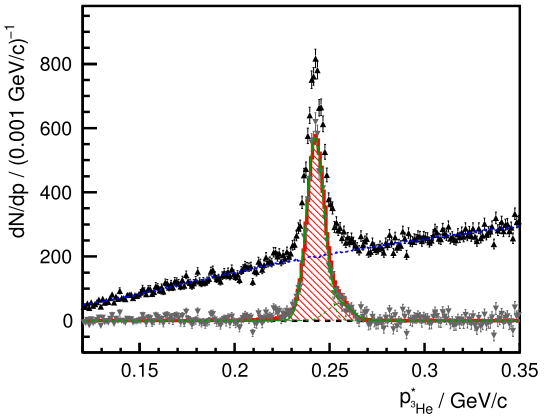

Fig. 2. Example of a background fit to the final state momentum spectrum of ^{3}He nuclei for $0.50 \le \cos\theta^*_\eta < 0.52$ at $p_p = 1.70$ GeV/c. Black triangles with black error bars represent measured data, the blue dashed line represents the estimated background, grey downward triangles with grey error bars show the same data, subtracted by the background expectation. The background subtracted signal is fitted by a double-Gaussian (green solid line), whose individual contributions are displayed by dashed green lines. The red histogram shows a MC simulation of the signal reaction $pd \to {}^3\mathrm{He}\,\eta$.

In order to determine the signal yield in a given bin in $\cos\theta^*_\eta$, the background subtracted data are summed over the interval $p^*_\eta - 3\sigma \le p^*_{^3\mathrm{He}} \le p^*_\eta + 3\sigma$, where p^*_η and σ are the position and width of the signal peak determined from a fit of an appropriate peak function to the background subtracted data. For most values of $\cos\theta^*_\eta$ a simple Gaussian is chosen. However, close to the maximum scattering angle the break-up of ^{3}He nuclei in the detector leads to asymmetric peaks (see Fig. 2) that are fitted by a double-Gaussian. In these cases, peak position and width of the dominant signal contribution are used.

Before physically meaningful angular distributions are obtained, the signal yield needs to be corrected for the product of detector acceptance and reconstruction efficiency, which can be derived from MC simulations. In contrast to earlier work [22], an extension to the GEANT3 software package [32] provided by the authors of [18] was used to simulate nuclear break-up of ^{3}He nuclei in the scintillator material. In addition, the possibility that the interaction occurs on the evaporated target gas rather than the pellet target was accounted for.

Simulations of the signal reaction $pd \to {}^3\mathrm{He}\,\eta$ were first performed with $\cos\theta^*_\eta$ equally distributed over all values from -1 to $+1$. From this set of simulations, the product of acceptance times reconstruction efficiency was calculated as the ratio of the number of events reconstructed in a bin of $\cos\theta^*_\eta$ divided by the number of events that were generated in that bin. However, only if the detector resolution were perfect would this ratio directly correspond to the sought-after product of acceptance and reconstruction efficiency. Otherwise, the finite detector resolution, in combination with a signal that exhibits a strong angular dependence, causes a bin migration effect in the opposite direction to the slope of the angular distribution. In addition, the nuclear break-up introduces a tendency to reconstruct the ^{3}He nuclei at slightly smaller kinetic energies. To account for these effects, the acceptance correction is done in an iterative manner. For this, the angular distributions observed in data, after correcting for the acceptance derived from the

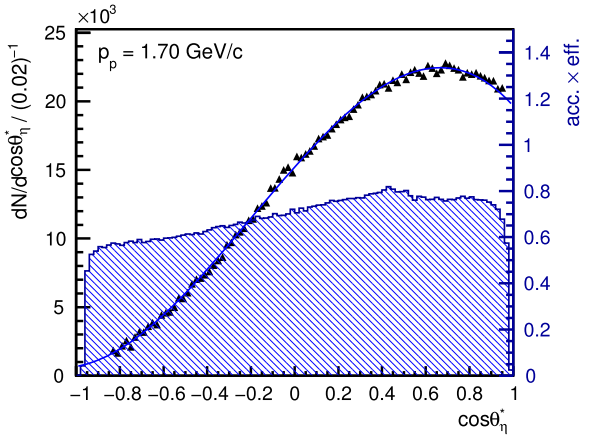

Fig. 3. Angular distribution of the reaction $pd \to {}^3\mathrm{He}\,\eta$ at $p_p = 1.70$ GeV/c. Black triangles represent data and the blue line a polynomial fit of the type given in Eq. (1). The shaded histogram displays the corresponding product of acceptance and reconstruction efficiency in each bin in $\cos\theta^*_\eta$, with the scale being displayed on the right hand axis. Only statistical uncertainties are shown.

MC sample equally distributed in $\cos\theta^*_\eta$, are fitted by a third order polynomial

$$f(\cos\theta^*_\eta) = N_0\left(1 + \alpha\cos\theta^*_\eta + \beta\cos^2\theta^*_\eta + \gamma\cos^3\theta^*_\eta\right). \qquad (1)$$

These polynomials are subsequently used to generate a new set of MC simulations with which the product of acceptance and reconstruction efficiency can again be determined. This procedure is repeated until convergence of all angular distributions is reached. The angular distribution, along with the product of acceptance and reconstruction efficiency of the sum of the three measurements at $p_p = 1.70$ GeV/c, is displayed in Fig. 3.

4. Normalization

For the measurement presented here, the normalization was carried out in two stages. The luminosity of the sum of the three measurements at $p_p = 1.70$ GeV/c ($Q_\eta = 61.7$ MeV) is determined by comparing the integral over the fit to the ${}^3\mathrm{He}\,\eta$ angular distribution displayed in Fig. 3 and the value of the total cross section $\sigma = (388.1 \pm 7.2_{\mathrm{stat.}})$ nb (with an additional 15% normalization uncertainty), measured by the ANKE collaboration at $Q_\eta = 60$ MeV [20]. The measurements at the 14 remaining beam momenta are then normalized relative to the luminosity derived for $p_p = 1.70$ GeV/c using proton–deuteron elastic scattering. Within experimental uncertainties, data in our energy and momentum-transfer range [33–37] suggest that the pd elastic differential cross section $d\sigma/dt$ is largely independent of the incident proton momentum p_p. In addition, as one of the objectives of this new measurement is to examine the cross section variation observed in [22], it is desirable to use a normalization method that is different from the single pion production $pd \to {}^3\mathrm{He}\,\pi^0$ used there.

Elastic pd scattering can be identified by demanding coincident charged particles in the forward and central detector and studying their angles. Since the forward-going protons are minimum ionizing, a measurement of their energy deposit does not help to determine their kinetic energy. A loose cut was first set on the azimuthal angles of the two tracks, $120° < |\varphi_{\mathrm{FD}} - \varphi_{\mathrm{CD}}| < 240°$, before comparing the polar angles of the two tracks. For a two-particle final state, the polar angles of both particles are directly related and this connection is evident in Fig. 4a for data corresponding to quasi-free $pd \to ppn_{\mathrm{spec}}$ and $pd \to pd$. In the case of proton–deuteron elastic scattering, the momentum transfer t is

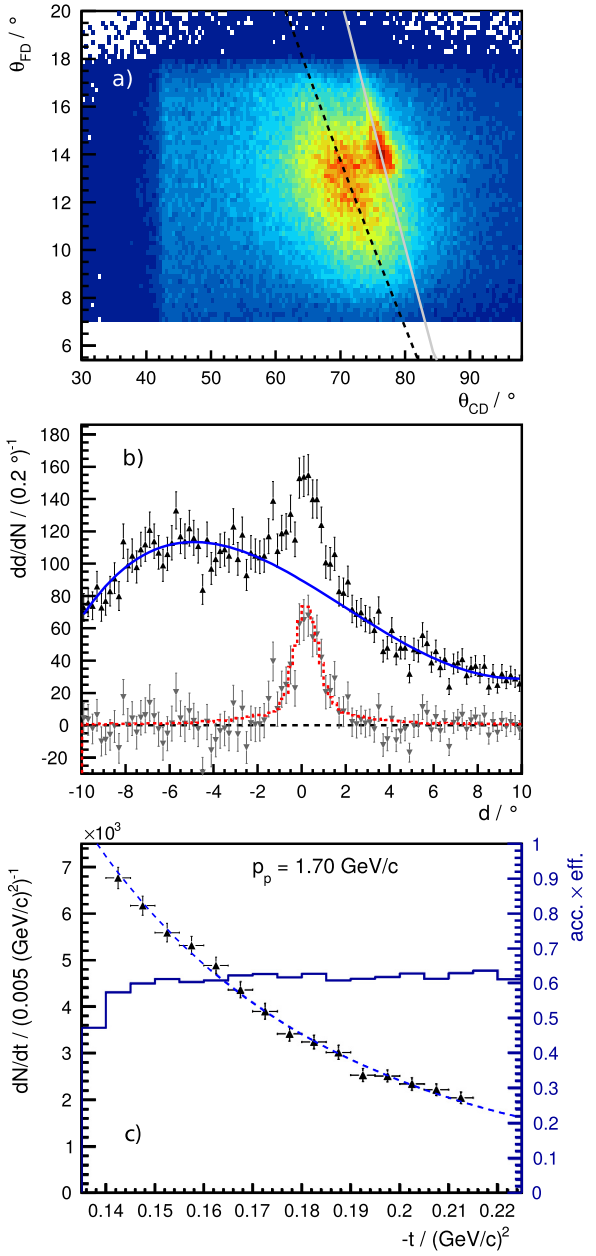

Fig. 4. a) Pairs of polar angles of coincidentally measured charged particles in the forward and central detectors, compared to the kinematical expectations for quasi-elastic $pd \to ppn_{\mathrm{spec}}$ scattering (black dotted line) and $pd \to pd$ elastic scattering (grey line). **b)** Projection onto the minimum distance d of a given pair of polar angles to the kinematic relation for pd elastic scattering, fitted by a fourth order polynomial (blue line). **c)** Distribution of pd elastic scattering events as a function of the momentum transfer t, fitted by a scaled fit to the literature data. The histogram represents the product of acceptance and reconstruction efficiency.

calculated from the proton polar angle. In addition, the minimum distance d to the kinematic expectation for pd elastic scattering is calculated for each pair of measured polar angles θ_{FD} and θ_{CD}. As seen from Fig. 4b, the distance d exhibits a narrow peak close to $d = 0$ for momentum transfers in the region $0.140\ (\mathrm{GeV}/c)^2 \le |t| \le 0.215\ (\mathrm{GeV}/c)^2$ on top of a strong background contribution due to quasi-elastic proton–proton scattering.

After excluding the signal region, the background in d is fitted by a fourth order polynomial and, after subtracting this, the acceptance-corrected event yield for proton–deuteron elastic scattering is determined as a function of $|t|$ for each beam momen-

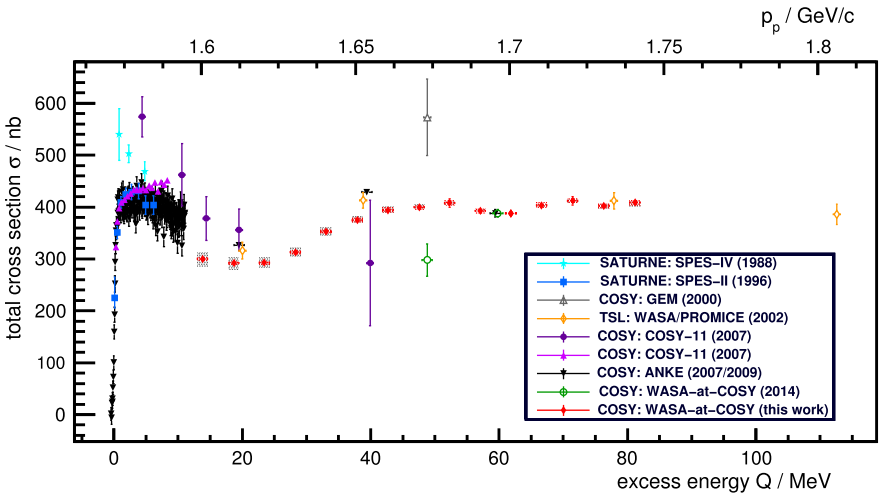

Fig. 5. Total cross section of the reaction $pd \to {}^3\mathrm{He}\,\eta$. Cyan stars are from [11], blue boxes from [12], grey open triangles from [21], orange open diamonds from [18], dark purple filled circles from [13], light purple upward filled triangles from [19], black downward filled triangles from [14,20], and green open circles from [22]. For the red filled diamonds from the present work, the error bars indicate the statistical point-to-point uncertainty, red boxes indicate the statistical chain-to-point uncertainty relative to the fixed cross section at $Q_\eta = 61.7$ MeV and grey boxes indicate the systematic uncertainty. In addition, a normalization uncertainty of 16.3% is to be understood. Similarly, the normalization uncertainties of the earlier data are also not displayed.

Table 2
Total cross section of the reaction $pd \to {}^3\mathrm{He}\,\eta$, including statistical point-to-point uncertainties $\Delta\sigma_{\mathrm{stat}}^{P2P}$, the uncertainty of the whole dataset relative to the fixed point at $Q_\eta = 61.7$ MeV $\Delta\sigma_{\mathrm{stat}}^{C2P}$, and the systematic uncertainties $\Delta\sigma_{\mathrm{sys}}^{\pm}$. The behaviour of the systematic uncertainty changes direction at $Q_\eta = 61.7$ MeV, as indicated by the sign. In addition, there is an overall normalization uncertainty of 16.3%.

Q_η in MeV	σ in nb	$\Delta\sigma_{\mathrm{stat}}^{P2P}$ in nb	$\Delta\sigma_{\mathrm{stat}}^{C2P}$ in nb	$\Delta\sigma_{\mathrm{sys}}^{-}$ in nb	$\Delta\sigma_{\mathrm{sys}}^{+}$ in nb
13.6(8)	300.3	6.5	3.4	−14.9	12.5
18.4(8)	292.2	5.8	3.3	−11.8	11.0
23.2(8)	292.8	5.8	3.3	−10.3	9.8
28.0(8)	312.9	6.0	3.5	−8.1	9.3
32.9(8)	352.6	7.0	4.0	−7.3	8.9
37.7(8)	374.7	7.3	4.2	−4.3	8.0
42.5(8)	394.0	8.0	4.4	−3.7	6.7
47.3(8)	399.8	7.6	4.5	−2.8	5.1
52.1(8)	408.0	8.1	4.6	−2.1	3.5
56.9(8)	392.7	7.2	4.4	−0.1	1.7
61.7(8)	388.1				
66.5(8)	403.3	7.8	4.5	2.6	−1.8
71.3(8)	412.0	8.4	4.6	2.8	−3.6
76.1(8)	402.5	7.7	4.5	3.3	−5.4
80.9(8)	408.7	7.9	4.6	2.3	−7.4

tum (see Fig. 4c). The combined database [33–37] can be fitted by $d\sigma/dt = \exp(12.45 - 27.24|t| + 26.31|t|^2)$, where t is measured in $(\mathrm{GeV}/c)^2$ [38], and this is scaled to the observed distribution dN/dt to determine the luminosity. There is good evidence that the pd elastic cross section $d\sigma/dt$ is largely independent of beam momentum in our kinematic region [39]. In this case the relative luminosity at two different momenta is directly given by the ratio of the two scaling factors.

5. Results

Our total cross sections at all 15 excess energies are given in Table 2 and displayed in Fig. 5, where they are compared to the data available in the literature. Since the cross section at $Q_\eta = 61.7$ MeV is fixed to the ANKE value [20], the statistical uncertainty of our measurement at that Q_η must be considered as a collective uncertainty $\Delta\sigma_{\mathrm{stat}}^{C2P}$ of our whole data set. In the supercycle mode, relative systematic effects, due to changes to the experimental or environmental conditions, can generally be ruled out. A careful study of the three measurements at $p_p = 1.70$ GeV/c shows no systematic changes between the data-taking periods. Systematic effects due to inefficiencies are also largely canceled out in the relative normalization. Uncertainty related to the ^{3}He break-up was estimated to be around 5% [18] but this is much reduced when using a relative normalization.

Two main sources of systematic uncertainty remain. The distribution and density of evaporated target gas in the scattering chamber is not known to high precision. As a shift of the vertex along the beam axis leads to a loss of information for large polar angles, variation of density and distribution in Monte Carlo simulations has implications on the geometrical acceptance. These are larger at higher Q_η when the maximum ^{3}He production angle is greater. Secondly, the assumption that the pd elastic scattering cross section $d\sigma/dt$ is constant as a function of the beam momentum, which is consistent with the precision of the available data, has been tested in model calculations [40,41]. These suggest that the integrated cross section over $0.140\ (\mathrm{GeV}/c)^2 \leq |t| \leq 0.215\ (\mathrm{GeV}/c)^2$ changes slightly but linearly with beam momentum. Relative to the value at $p_p = 1.70$ GeV/c, this would change the luminosity by $\approx 4\%$ at $p_p = 1.60$ GeV/c and -2% at $p_p = 1.74$ GeV/c. Both these systematic uncertainties are asymmetric and Gaussian error propagation leads to the values of $\Delta\sigma_{\mathrm{sys}}^{-}$ and $\Delta\sigma_{\mathrm{sys}}^{+}$ given in Table 2. Here, the sign in $\Delta\sigma_{\mathrm{sys}}^{\pm}$ indicates the sign of the systematic uncertainty at the smallest energy. Due to the relative normalization, the systematic uncertainty changes sign when crossing the reference momentum $p_p = 1.70$ GeV/c.

In addition, the overall normalization factor from the comparison of the $Q_\eta = 61.7$ MeV data with the total cross section published in [20] comes with an uncertainty of 16.3%. Of this, 15% is associated with the literature cross section and an additional 6.3% uncertainty was found when different subparts of the differential cross section were used for normalization instead of the total cross section. These 16.3% are, however, irrelevant when discussing the energy dependence of the total cross section.

From Fig. 5, it is apparent that the abrupt change in the total cross section between 40 and 50 MeV, that was previously reported in [22], is not confirmed by the present analysis. However, by repeating the normalization procedure used in [22] on

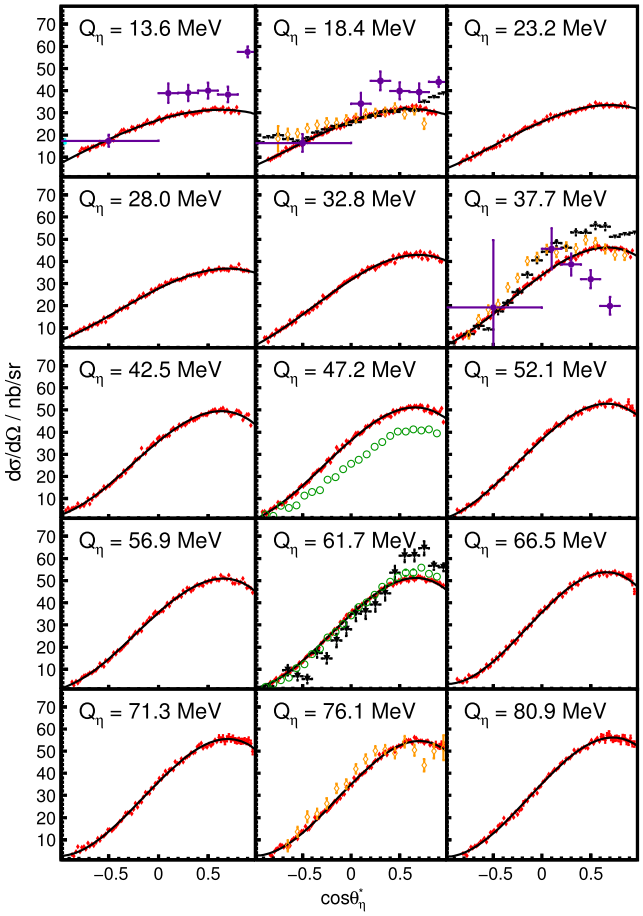

Fig. 6. Differential cross sections of the reaction $pd \to {}^3\mathrm{He}\,\eta$ at 15 excess energies between $Q_\eta = 13.6$ MeV and $Q_\eta = 80.9$ MeV. The black line represents a fit of a third order polynomial as given in Eq. (1). Wherever possible, earlier data are shown for comparison, using the same colour code as in Fig. 5. Data from [21] are omitted due to their large uncertainties.

the present data, it could be shown that the anomalous behaviour was due to an incorrect assumption regarding the differential cross section for single pion production rather than an error in the measurement itself [42]. In reality the backward cross section for $pd \to {}^3\mathrm{He}\,\pi^0$ has a minimum in the energy region of interest and the variation with energy is very strong [43].

In the excess energy interval 20 MeV $\lesssim Q_\eta \lesssim$ 60 MeV, the increase and subsequent leveling off of the total cross section, that was observed in [18,20], is also seen in the present work. It can, however, be studied in a lot more detail than was previously possible.

The differential cross sections derived in the present work are displayed in Fig. 6. Generally, the distributions at all energies exhibit the forward-peaking that was observed in other experiments, though the maxima are typically at $\cos\theta \approx 0.7$ rather than in the forward direction. Due to the large amount of data gathered, the angular distributions as well as their energy dependence can be studied in unprecedented detail. At all energies, the differential cross sections can be well described by the third order polynomial of Eq. (1) and the values of the fit parameters are given in Tables 3–5. The error bars shown there were discussed earlier in this section.

The asymmetry parameter α is of special importance, as it is often used to study the interference between s- and p-waves in the near-threshold data (see, e.g., [14,16]), which might reflect the influence of η-mesic states below threshold. In Fig. 7, the values at the three lowest energies of the present work are compared to published asymmetry parameters [14,20,13]. The agreement with the higher values from COSY-11 [13] might be slightly preferred compared to the ANKE results [14]. The ANKE value at $Q_\eta = 19.5$ MeV is in strong conflict to the findings reported here, but, as already argued in [20], the inclusion of this point into a

Table 3
Values of the fit parameter N_0 of Eq. (1) at all 15 excess energies.

Q_η in MeV	N_0 in nb/sr	$\Delta N_{0,\mathrm{stat}}$ in nb/sr	$\Delta N^-_{0,\mathrm{sys}}$ in nb/sr	$\Delta N^+_{0,\mathrm{sys}}$ in nb/sr
13.6(8)	26.81	0.46	0.84	0.20
18.4(8)	26.22	0.40	0.54	0.15
23.2(8)	25.96	0.40	0.30	0.15
28.0(8)	27.72	0.44	0.17	0.10
32.9(8)	31.68	0.58	0.17	0.17
37.7(8)	33.78	0.64	0.21	0.51
42.5(8)	35.77	0.74	0.14	0.62
47.3(8)	36.29	0.71	0.14	0.72
52.1(8)	36.72	0.77	0.14	0.67
56.9(8)	35.49	0.67	0.14	0.84
61.7(8)	34.71	0.63	0.12	0.75
66.5(8)	35.68	0.72	0.13	0.96
71.3(8)	36.02	0.78	0.12	0.94
76.1(8)	35.03	0.70	0.13	0.97
80.9(8)	35.29	0.72	0.18	0.83

Table 4
Values of the fit parameter α of Eq. (1) at all 15 excess energies.

Q_η in MeV	α	$\Delta\alpha_{\mathrm{stat}}$	$\Delta\alpha^-_{\mathrm{sys}}$	$\Delta\alpha^+_{\mathrm{sys}}$
13.6(8)	0.517	0.017	0.012	0.015
18.4(8)	0.619	0.014	0.009	0.018
23.2(8)	0.736	0.015	0.009	0.022
28.0(8)	0.804	0.014	0.011	0.023
32.9(8)	0.894	0.014	0.008	0.026
37.7(8)	0.948	0.013	0.010	0.023
42.5(8)	1.025	0.014	0.008	0.022
47.3(8)	1.054	0.013	0.008	0.026
52.1(8)	1.101	0.013	0.009	0.027
56.9(8)	1.118	0.013	0.007	0.022
61.7(8)	1.183	0.008	0.009	0.023
66.5(8)	1.253	0.014	0.009	0.022
71.3(8)	1.257	0.014	0.008	0.017
76.1(8)	1.285	0.014	0.008	0.020
80.9(8)	1.306	0.015	0.008	0.017

Table 5
Values of the fit parameters β and γ of the function given Eq. (1) at all 15 excess energies. Systematic uncertainties omitted here can be found in [42].

Q_η in MeV	β	$\Delta\beta_{\mathrm{stat}}$	γ	$\Delta\gamma_{\mathrm{stat}}$
13.6(8)	−0.326	0.016	−0.098	0.041
18.4(8)	−0.339	0.012	−0.180	0.028
23.2(8)	−0.307	0.012	−0.213	0.030
28.0(8)	−0.305	0.012	−0.255	0.028
32.9(8)	−0.343	0.011	−0.296	0.027
37.7(8)	−0.352	0.011	−0.356	0.026
42.5(8)	−0.371	0.011	−0.463	0.026
47.3(8)	−0.370	0.010	−0.438	0.024
52.1(8)	−0.347	0.011	−0.480	0.025
56.9(8)	−0.358	0.010	−0.511	0.024
61.7(8)	−0.331	0.010	−0.560	0.016
66.5(8)	−0.302	0.011	−0.652	0.026
71.3(8)	−0.269	0.012	−0.599	0.027
76.1(8)	−0.257	0.012	−0.624	0.029
80.9(8)	−0.235	0.013	−0.605	0.031

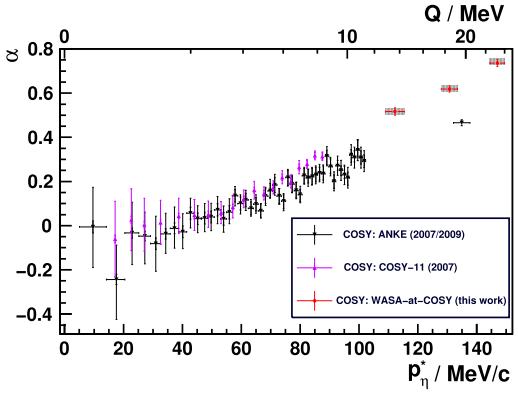

Fig. 7. Asymmetry parameter α of the angular distributions of the reaction $pd \to {}^3\mathrm{He}\,\eta$. Systematic uncertainties of the present data (red diamonds) are shown as grey boxes. For the earlier data from ANKE [14,20] (black downward triangles) and COSY11 [13] (purple upward triangles) thick lines represent statistical uncertainties, thin lines systematic ones.

combined fit with the data from [14] yields an unsatisfactory result.

6. Summary

In the course of this work, total and differential cross sections of the η meson production in proton–deuteron fusion were extracted. The differential distributions exhibit the same forward-peaking behaviour as previously observed away from the reaction threshold. Due to the amount and quality of the data, it is possible for the first time to study changes in the shape of the angular distributions with rising excess energy over a large interval between 13.6 MeV and 80.9 MeV. In this way, the contributions of higher partial waves might be studied. This will greatly aid in the investigation of the production process, which is poorly understood.

A sharp variation of the total cross section around $Q_\eta \approx 50$ MeV, that was previously reported [22], is not confirmed. However, the oscillating structure of the production cross section between $Q_\eta \approx 10$ MeV and $Q_\eta \approx 60$ MeV that had already been observed by both the WASA/PROMICE and ANKE experiments [18, 20], albeit in much less detail, is nicely reproduced. Close to the production threshold, effects of a strong final state interaction are thought to be a dominating factor in the energy dependence of the total cross section. The observed structure reported here might indicate the energy region in which the final state interaction loses its importance. With none of the available theoretical models being able to reproduce the forward-peaking in the angular distributions (see, e.g., [26,28]) as well as the observed total cross section, further theoretical effort is clearly needed in order to fully understand the production of η mesons in association with ^{3}He nuclei.

Acknowledgements

The present work received funding from the European Union Seventh Framework Programme (FP7/2007-2013) under grant agreement number 283286. We gratefully acknowledge the support given by the Forschungszentrum Jülich Centre for Hadron Physics of the FFE Funding Programme, by the Polish National Science Centre through the grant No. 2016/23/B/ST2/00784, and by the DFG through the Research Training Group GRK2149. We thank the COSY crew for their work and the excellent conditions during the beam time and Dr. M. N. Platonova and Dr. V I. Kukulin for their valuable contributions regarding proton–deuteron elastic scattering.

References

[1] R.S. Bhalerao, L.C. Liu, Phys. Rev. Lett. 54 (1985) 865–868, https://doi.org/10.1103/PhysRevLett.54.865.
[2] Q. Haider, L.C. Liu, Phys. Lett. B 172 (1986) 257–260, https://doi.org/10.1016/0370-2693(86)90846-4.
[3] H. Calen, et al., Phys. Rev. Lett. 79 (1997) 2642–2645, https://doi.org/10.1103/PhysRevLett.79.2642.
[4] H. Calen, et al., Phys. Rev. Lett. 80 (1998) 2069–2072, https://doi.org/10.1103/PhysRevLett.80.2069.
[5] R. Bilger, et al., Phys. Rev. C 69 (2004) 014003, https://doi.org/10.1103/PhysRevC.69.014003.
[6] Daniel Schröer, Christopher Fritzsch, Alfons Khoukaz, Marcel Rump, ANKE, EPJ Web Conf. 130 (2016) 03008, https://doi.org/10.1051/epjconf/201613003008.
[7] R. Frascaria, et al., Phys. Rev. C 50 (1994) R537–R540, https://doi.org/10.1103/PhysRevC.50.R537.
[8] A. Wronska, et al., Eur. Phys. J. A 26 (2005) 421–428, https://doi.org/10.1140/epja/i2005-10185-0, arXiv:nucl-ex/0510056.
[9] M. Pfeiffer, et al., Phys. Rev. Lett. 92 (2004) 252001, https://doi.org/10.1103/PhysRevLett.92.252001, arXiv:nucl-ex/0312011.
[10] F. Pheron, et al., Phys. Lett. B 709 (2012) 21–27, https://doi.org/10.1016/j.physletb.2012.01.075, arXiv:1201.6517.
[11] J. Berger, et al., Phys. Rev. Lett. 61 (1988) 919–922, https://doi.org/10.1103/PhysRevLett.61.919.
[12] B. Mayer, et al., Phys. Rev. C 53 (1996) 2068–2074, https://doi.org/10.1103/PhysRevC.53.2068.
[13] J. Smyrski, et al., Phys. Lett. B 649 (2007) 258–262, https://doi.org/10.1016/j.physletb.2007.04.021, arXiv:nucl-ex/0702043.
[14] T. Mersmann, et al., Phys. Rev. Lett. 98 (2007) 242301, https://doi.org/10.1103/PhysRevLett.98.242301, arXiv:nucl-ex/0701072.
[15] C. Wilkin, Phys. Rev. C 47 (1993) R938, https://doi.org/10.1103/PhysRevC.47.R938, arXiv:nucl-th/9301006.
[16] C. Wilkin, et al., Phys. Lett. B 654 (2007) 92–96, https://doi.org/10.1016/j.physletb.2007.08.041, arXiv:0707.1489.
[17] J.-J. Xie, W.-H. Liang, E. Oset, P. Moskal, M. Skurzok, C. Wilkin, Phys. Rev. C 95 (2017) 015202, https://doi.org/10.1103/PhysRevC.95.015202, arXiv:1609.03399.
[18] R. Bilger, et al., Phys. Rev. C 65 (2002) 044608, https://doi.org/10.1103/PhysRevC.65.044608.
[19] H.-H. Adam, et al., Phys. Rev. C 75 (2007) 014004, https://doi.org/10.1103/PhysRevC.75.014004.
[20] T. Rausmann, et al., Phys. Rev. C 80 (2009) 017001, https://doi.org/10.1103/PhysRevC.80.017001, arXiv:0905.4595.
[21] M. Betigeri, et al., GEM, Phys. Lett. B 472 (2000) 267–272, https://doi.org/10.1016/S0370-2693(99)01456-2, arXiv:nucl-ex/9912006.
[22] P. Adlarson, et al., WASA-at-COSY, Eur. Phys. J. A 50 (2014) 100, https://doi.org/10.1140/epja/i2014-14100-4, arXiv:1402.3469.
[23] N.G. Kelkar, et al., Rep. Prog. Phys. 76 (2013) 066301, https://doi.org/10.1088/0034-4885/76/6/066301, arXiv:1306.2909.
[24] K. Kilian, H. Nann, AIP Conf. Proc. 221 (1991) 185–191, https://doi.org/10.1063/1.40356.
[25] G. Fäldt, C. Wilkin, Nucl. Phys. A 587 (1995) 769–786, https://doi.org/10.1016/0375-9474(95)00074-B.
[26] K.P. Khemchandani, N.G. Kelkar, B.K. Jain, Phys. Rev. C 68 (2003) 064610, https://doi.org/10.1103/PhysRevC.68.064610, arXiv:nucl-th/0311029.
[27] K.P. Khemchandani, et al., Phys. Rev. C 76 (2007) 069801, https://doi.org/10.1103/PhysRevC.76.069801, arXiv:0712.1993.
[28] A.B. Santra, et al., Phys. Rev. C 64 (2001) 025201, https://doi.org/10.1103/PhysRevC.64.025201.
[29] H.-H. Adam, et al., WASA-at-COSY, arXiv:nucl-ex/0411038, 2004.
[30] R. Maier, Nucl. Instrum. Methods A 390 (1997) 1–8, https://doi.org/10.1016/S0168-9002(97)00324-0.
[31] P. Adlarson, et al., WASA-at-COSY, Phys. Rev. C 91 (2015) 015201, https://doi.org/10.1103/PhysRevC.91.015201, arXiv:1408.5744.
[32] R. Brun, et al., https://cds.cern.ch/record/1082634/files/geantall_CERN-W5013.pdf, 1994.
[33] N. Dalkhazhav, et al., Sov. J. Nucl. Phys. 8 (1969) 196–202, Yad. Fiz. 8 (1968) 342.
[34] E. Winkelmann, et al., Phys. Rev. C 21 (1980) 2535–2541, https://doi.org/10.1103/PhysRevC.21.2535.
[35] F. Irom, et al., Phys. Rev. C 28 (1983) 2380–2385, https://doi.org/10.1103/PhysRevC.28.2380.
[36] G.N. Velichko, et al., Sov. J. Nucl. Phys. 47 (1988) 755–759, Yad. Fiz. 47 (1988) 1185.
[37] E. Guelmez, et al., Phys. Rev. C 43 (1991) 2067–2076, https://doi.org/10.1103/PhysRevC.43.2067.
[38] M. Mielke, et al., Eur. Phys. J. A 50 (2014) 102, https://doi.org/10.1140/epja/i2014-14102-2, arXiv:1404.2066.
[39] C. Fritzsch, M.N. Platonova, V.I. Kukulin, 2017, publication in preparation, private communication.

[40] M.N. Platonova, V.I. Kukulin, Phys. Rev. C 81 (2010) 014004, https://doi.org/10.1103/PhysRevC.81.014004, arXiv:1612.08694, Erratum: Phys. Rev. C 94 (6) (2016) 069902, https://doi.org/10.1103/PhysRevC.94.069902.
[41] M.N. Platonova, V.I. Kukulin, 2017, private communication.
[42] N. Hüsken, η and π^0 Production in Proton–Deuteron Fusion to ^{3}HeX with WASA-at-COSY, Ph.D. thesis, Westfälische Wilhelms-Universität Münster, 2017.
[43] C. Kerboul, et al., Phys. Lett. B 181 (1986) 28–32, https://doi.org/10.1016/0370-2693(86)91248-7.